The Chaotic Pendulum

Tasha Arvanitis and Vivian Steyert

12 December 2012

Abstract

The behavior of the chaotic pendulum in the Sophomore Lab is investigated. In the undamped, undriven case, small oscillations are observed. With increasing drive frequency, the behavior becomes chaotic, and a region of period doubling is present at frequencies just above the chaotic regime. Both the onset of chaos and the general shape of Poincaré plots are similar to those observed in the physical system.

1 Introduction

A behavior of a chaotic pendulum is investigated. The system consists of an aluminum disk with uniformly-distributed mass M and radius R, to which is attached an eccentric mass of mass m, at the edge of the disk. The setup is shown in Figure 1. There is a permanent magnet held close to the disk, which generates eddy currents and thus produces a (hopefully) linear damping force. The disk is attached to a pulley of radius r, which has a string wrapped around it in such a way as to avoid slipping. This string is attached to a spring on each side. The spring on the left side has a spring constant k_1, and the one on the right has a spring constant k_2. The far end of spring 2 is fixed. Finally, the whole system is driven by means of a rotary motor fixed to the end of spring 1, which drives the spring according to $De^{-i\omega t}$.

2 Equation of Motion

We will use a single generalized coordinate θ, which will describe the angle between the vertical and the eccentric mass. We define θ to be zero when the eccentric mass is at the top of the disk, and to be positive in the clockwise direction (also shown in Figure 1).

Observe that the moment of inertia I is

$$I = \frac{1}{2}MR^2 + mR^2.$$

Thus the kinetic energy of the system is

$$T = \frac{1}{2} I \dot{\theta}^2 = \frac{1}{2} \left(\frac{1}{2} M R^2 + m R^2 \right) \dot{\theta}^2.$$

The potential energy of the system is the sum of the gravitational and spring potential energies. Define the stretch of the springs when the eccentric mass is in unstable equilibrium at the top of the disk to be x_1 and x_2, respectively. Then the potential energy of the system is

$$U = mgR\cos\theta + \frac{1}{2} k_1 \left(x_1 + r\theta - De^{-i\omega t} \right)^2 + \frac{1}{2} k_2 \left(x_2 - r\theta \right)^2.$$

In general, we have used $De^{-i\omega t}$ to describe the drive, but in our model, we used the imaginary part of this complex exponential. This was in order to have the drive be in neutral position at the starting time, which matches the data collection on the physical apparatus. We took the drive to be entirely in a line, rather than in a circle as in the physical system. We also treated the springs as ideal.

At any equilibrium position, $U'(\theta)$ is zero. Examination of $U'(\theta)$ at the

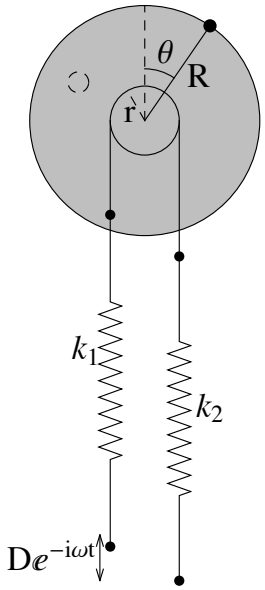

Figure 1: The chaotic pendulum under investigation. The dashed circle represents the permanent magnet for damping. The bottom end of spring 2 is fixed, while the bottom end of spring one is driven sinusoidally.

unstable equilibrium at the top of the disk yields

$$\begin{aligned} U'(\theta) &= mgR\sin\theta - k_1 r\left(x_1 + r\theta - De^{-i\omega t}\right) + k_2 r\left(x_2 - r\theta\right) \\ U'(0) &= -k_1 x_1 + k_2 x_2 = 0 \\ k_1 x_1 &= k_2 x_2. \end{aligned}$$

Here the drive has been omitted, as we take it to be at the center of its displacement when the apparatus is balanced.

Note that the potential and kinetic energies do not account for damping. This will be addressed shortly. The Lagrangian (sans damping) is

$$L = \frac{1}{2}I\dot{\theta}^2 - mgR\cos\theta - \frac{1}{2}k_1\left(x_1 + r\theta - De^{-i\omega t}\right)^2 - \frac{1}{2}k_2\left(x_2 - r\theta\right)^2.$$

Euler's equation shows

$$\begin{aligned} \mathbf{F}\cdot\frac{\partial\mathbf{r}}{\partial\theta} &= \frac{d}{dt}\frac{\partial L}{\partial\dot{\theta}} - \frac{\partial L}{\partial\theta} \\ -c\dot{\theta} &= I\ddot{\theta} - \left(mgR\sin\theta - k_1 r\left(x_1 + r\theta - De^{-i\omega t}\right) + k_2 r(x_2 - r\theta)\right). \end{aligned}$$

The left-hand term is $-c\dot{\theta}$ because the external force from the damper will eventually end up being proportional to the speed of rotation. This c does *not* correspond to the damping coefficient for the eddy-current damper. The whole term is negative because the damping always opposes the motion of the system. We assume that the damping from the magnet overwhelms the effect of friction, which we have ignored.

The relationship between the spring constants and x_i's simplifies the equation of motion to

$$-c\dot{\theta} = I\ddot{\theta} - mgR\sin\theta + (k_1 + k_2)r^2\theta - k_1 rDe^{-i\omega t}.$$

This is the equation of motion for the system.

This equation can be made dimensionless by defining $\omega_0 = \sqrt{g/R}$ and $\mathcal{T} = \omega_0 t$. Algebraic manipulation yields the dimensionless equation

$$\begin{aligned} \theta'' + \frac{c}{\left(\frac{1}{2}M + m\right)R^2\omega_0}\theta' - \frac{mg}{\left(\frac{1}{2}M + m\right)R\omega_0^2}\sin\theta \\ + \frac{(k_1 + k_2)r^2}{\left(\frac{1}{2}M + m\right)R^2\omega_0^2}\theta = \frac{k_1 rD}{\left(\frac{1}{2}M + m\right)R^2\omega_0^2}e^{-i\frac{\omega}{\omega_0}\mathcal{T}}. \end{aligned}$$

This is the dimensionless equation of motion for the system. However, we hope to compare the behavior we predict based on the equation of motion with the observed behavior of the system, and this comparison will be more explicit if we instead use real (dimension-ful) time.

3 System parameters

Our project is based on a physical system that is sitting in the Sophomore Lab space downstairs. As such, we fixed most of our constants to match the parameters of that system. We made this decition in order to compare theoretical predictions with experimental results. Our parameters are:

Mass of disk	M	0.120 kg
Eccentric mass	m	0.01454 kg
Radius of disk	R	0.0475 m
Radius of pulley	r	0.024 m
Left spring constant	k_1	3.12 N/m
Right spring constant	k_2	3.13 N/m
Acceleration due to gravity	g	9.81 m/s^2
Damping constant	c	0.0001 kg m/s
Drive amplitude	D	0.0254 m

where the damping constant was chosen somewhat arbitrarily. We chose the value of c based on approximate behavior of the system; that is with chaotic behavior beginning and ending between 0 and 1 Hz. The drive amplitude of the physical system can be varied. Unless otherwise noted, we have used $D = 0.0254$ m in this report. The parameter we will vary in most of this investigation is the drive frequency, ω.

4 Results

4.1 Equilibrum and Small Oscillations

The system, as one might gather from physical intuition, has an unstable equilibrium position with the eccentric mass vertical, and two stable equilibrium positions, one on each side. Graphing the potential energy as a function of θ, with no drive amplitude, agrees with expectations, as shown in Figure 2. The potential energy increases as we wind the pendulum up further, with small dips as the height, and potential energy due to gravity, fluctuate.

The equilibrium angles can be calculated based on our physical quantities; they are the values of θ that solve

$$(k_1 + k_2)r^2\theta = mgR\sin(\theta),$$

which in our setup are ± 1.82265 radians (and zero). The equilibrium point at $\theta = 0$ is unstable, while the other two are the points of lowest potential energy and are thus stable. We expect that oscillation will be around one of these stable equilibrium positions or switching between them.

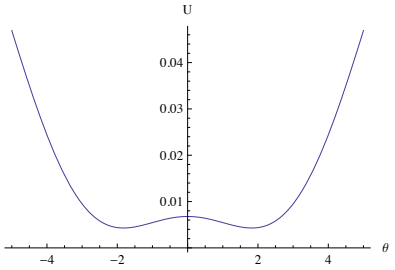

(a) Potential wells for small values of θ.

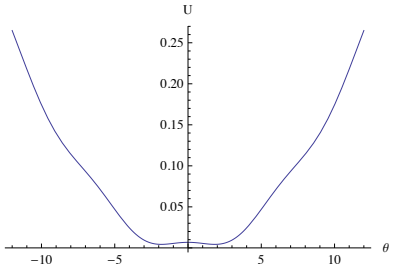

(b) Potential wells for larger values of θ.

Figure 2: Potential energy as a function of angular position

For small oscillations, we expect the mass to stay in one of the potential wells, exhibiting simple periodic motion. By setting the damping term and drive amplitude to zero, we can investigate a simplified version of this system. As shown in Figure 3, a small displacement from the stable equilibrium in either potential well results in motion that looks a lot like simple harmonic oscillation.

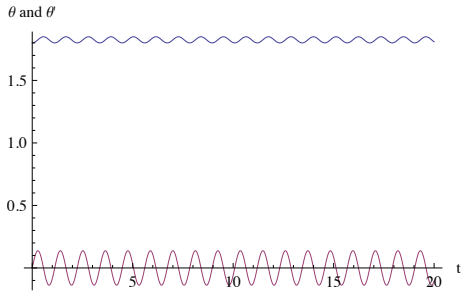

Figure 3: Angular position (blue) and velocity (red) as a function of time for a small initial displacement from equilibrium without damping or drive.

4.2 General Behavior

Adding damping and drive, of course, makes the system more interesting. Figure 4 shows some time traces of the motion for different drive frequencies. At low frequencies, the eccentric mass stays in one well with complicated but periodic behavior. As we increase frequency, we encounter some regions where the mass periodically switches between positive and negative θ, regions where it stays in one potential well, and eventually, we encounter a region of chaotic motion. At the highest frequencies the physical system is built for (around 1 Hz), the system goes back to periodic motion in one well.

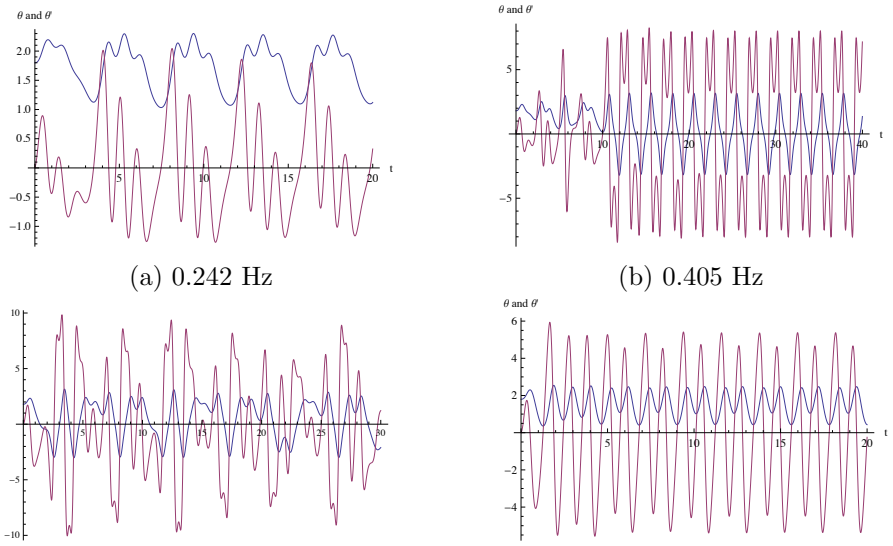

(a) 0.242 Hz (b) 0.405 Hz

(c) 0.762 Hz (d) 0.910 Hz

Figure 4: Angular position (blue) and velocity (red) for drive frequencies: 0.242 Hz (a), 0.405 Hz (b), 0.762 Hz (c), and 0.910 Hz (d). The third of these shows chaos while the others are various types of periodic behavior.

4.3 Phase plots

The chaotic pendulum system may be viewed as traveling through the three-dimensional phase space defined by the phase of the drive and the eccentric mass's angular position and velocity. The system is completely deterministic, so if its location in phase space at a starting time is known, its behavior can be predicted for all time. This means that if the path traced out by the system in phase space crosses itself, it is bound to repeat periodically in a closed loop.

A useful way of visualizing the motion of the system is using a phase plot, which shows the bob's angular velocity with respect to its angular position. After an initial transient is allowed to die out, any periodic behavior will be seen as a closed loop. An example of a phase plot of periodic behavior is shown in part (a) of Figure 5.

Nonperiodic behavior leads to a more dynamic phase plot. An example phase plot of nonperiodic behavior is shown in part (b) of Figure 5. Note that the path can cross itself without becoming periodic because this two-dimensional phase plot leaves out the phase of the drive, which is required in order to fully describe the system's behavior.

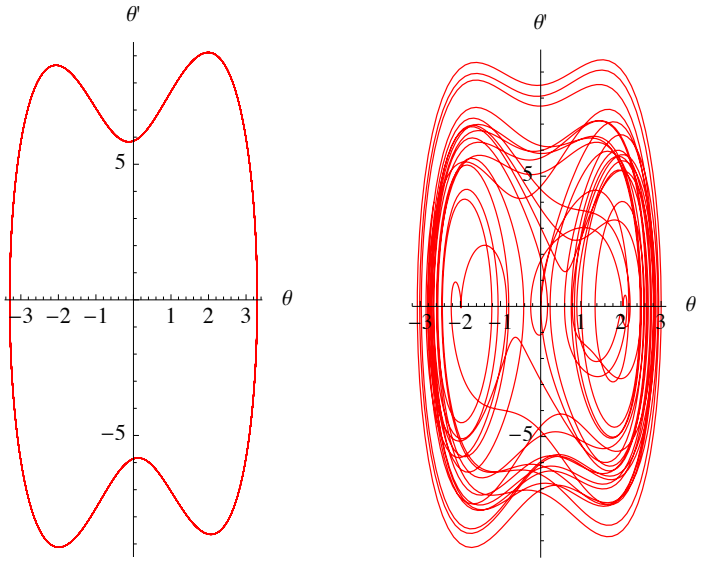

(a) Periodic behavior (b) Nonperiodic behavior

Figure 5: Phase plot of the chaotic pendulum system. The plot shown in (a) uses a driving frequency of 0.500 Hz and starts plotting after the transient behavior has died out. It shows that the bob oscillates periodically between the two potential wells. The plot shown in (b) uses a driving frequency of 0.700 Hz and exhibits nonperiodic behavior.

4.4 Poincaré plots

Phase plots are useful for examining system behavior over short periods of time, but tend to get cluttered over longer runs. In such cases, a Poincaré plot can be used to examine the system's behavior. Poincaré plots have the same axes as phase plots, but the position and velocity data are only taken once per drive cycle. Thus, if the behavior is periodic with frequency equal to the drive frequency, we expect our Poincaré plot to show a single dot — the system comes back to the same state after each drive period. For chaotic motion, we expect many dots, as the motion is not really periodic so the drive period will end with the system in a wide variety of states. Figure 6 shows Poincaré plots for several frequencies.

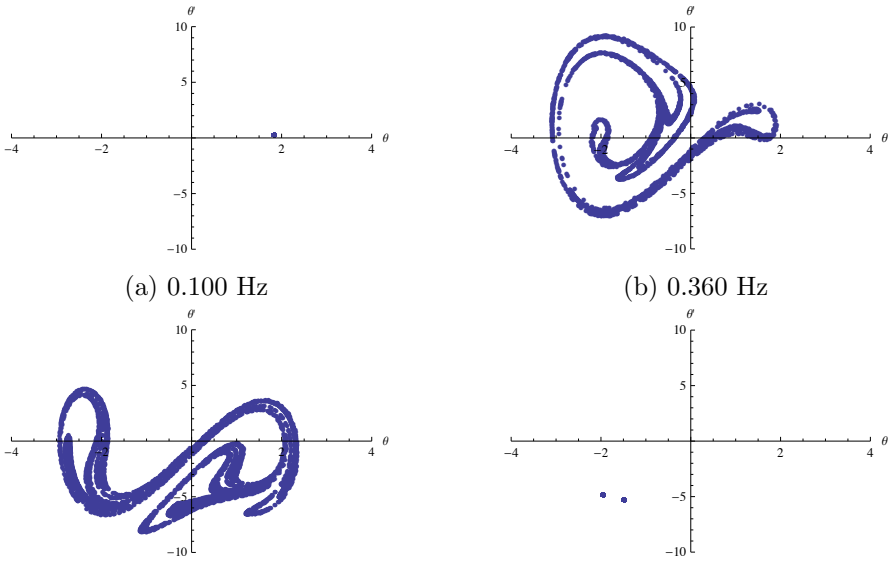

(a) 0.100 Hz

(b) 0.360 Hz

(c) 0.858 Hz

(d) 0.920 Hz

Figure 6: Poincare plots for a variety of frequencies. Part (a) is a plot of a frequency for which the system exhibits periodic behavior with a single period. Part (d) is a plot of a frequency for which the system exhibits period doubling. Parts (b) and (c) show Poincaré plots of chaotic behavior.

4.5 Bifurcation diagrams

Bifurcation diagrams can be used in order to get a large-scale understanding of a system. They show a set of points from Poincaré plots at a range of frequencies and can give a good idea of boundaries of chaos, as well as regions of period doubling. The large-scale bifurcation diagram and a zoomed version of a region of period doubling are shown in Figure 10 at the end of the report.

From the large-scale plot we see that the main chaotic region occurs at frequencies between about 0.65 Hz to 0.86 Hz. At frequencies immediately below the lower end of this chaotic behavior the system behaves periodically with only one period, before which it exhibits some regional periodic and chaotic behavior. At frequencies just above the primary chaotic boundary, there is a region of bifurcation (shown in part (b) of Figure 10).

This region of bifurcation contains successive 'forks' at which the number of drive periods in a period of the system doubles. The frequencies at which these forks occur is theoretically related by the first Feigenbaum constant, which is defined as the ratio

$$\frac{f_{n-1} - f_{n-2}}{f_n - f_{n-1}}$$

where f_i is the frequency of the i^{th} fork. It has a value of $\delta \approx 4.669$, independent of the chaotic system under investigation. The detailed bifurcation plot was examined to find approximate values for f_1 through f_4 of

f_1	0.926 ± 0.002 Hz
f_2	0.902 ± 0.002 Hz
f_3	0.898 ± 0.002 Hz
f_4	0.897 ± 0.002 Hz

The uncertainties on these values are large because we found the bifurcation frequencies by eyeballing the bifurcation plot. While we attempted to find the branching frequencies more accurately, the 'clutter' in the bifurcation region made this very difficult.

Based on these values, Feigenbaum's first constant was calculated as 6.0 ± 4.3 for $n = 3$. While the uncertainty on this number is large for the reasons discussed above, it should still be noted that the true value of the first constant falls squarely in the ranges for the 'experimental' value.

5 Comparison to Experiment

Since we have access to the physical system modeled in this report, some limited comparisons could be made between what our model predicts and what we observed experimentally. As mentioned previously, most parameters should be the same in experiment and model, so we expect there to be

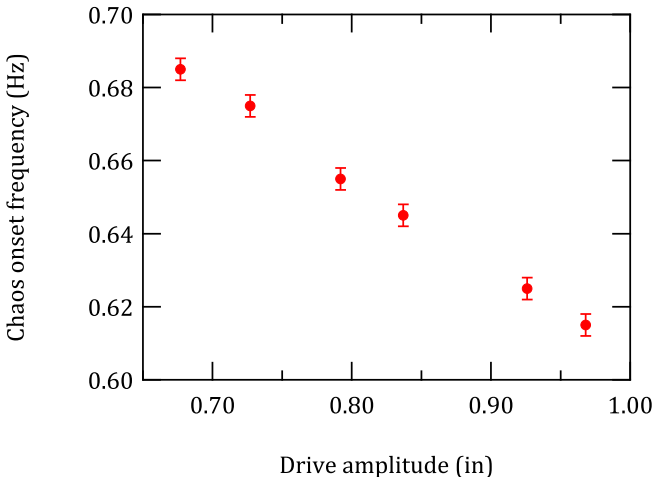

(a) Physical observations

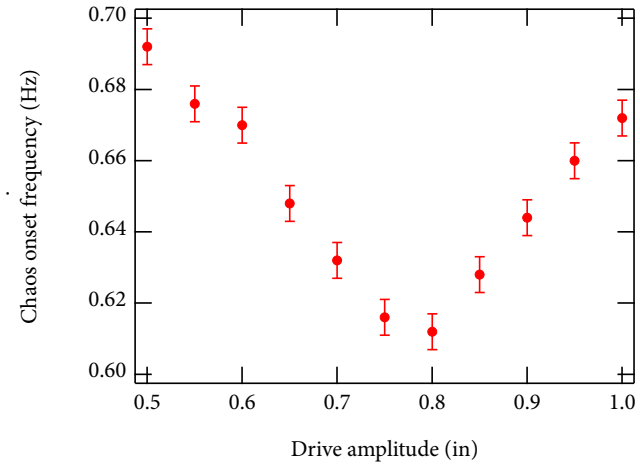

(b) Theoretical predictions

Figure 7: Plots of the frequencies at which chaotic behavior begins in the (a) physical and (b) theoretical systems. The trends seem to be offset by an amplitude of about 0.2 to 0.3 inches, which can be adjusted by changing the damping constant.

substantial correlation between experimental and theoretical results.

5.1 Onset of Chaos

A benefit of the bifurcation plot is the ease with which the frequency at which chaos begins can be identified. In part (a) of Figure 10, the onset of chaos is the frequency at which the dense region begins, around 0.672 Hz.

While it is easy to identify the approximate onset of chaos by just 'eyeballing' the bifurcation plots, it is difficult to find a unique onset of chaos using a script, because the lower chaotic boundary is itself chaotic. For the purposes of the plots below, the 'onset' was taken to be the first non-isolated vertical band in the bifurcation plot, to within 0.001 Hz.

The onsets of chaos in our theoretical predictions compare closely with the experimental values for the onset of chaos. Rough plots comparing the frequencies at which chaos begins in the physical system (a) and the predictions from our model (b) are shown in Figure 7. The frequencies at which chaos begins are similar between theory and experiment, but the drive amplitudes at which these frequencies of onset occur are slightly offset.

This difference can largely be accounted for by changing our damping constant. Choosing $c = 0.00015$ kg m/s yields the chaos onset plot shown in Figure 8. This new plot is more in line with the trend determined experimentally, but the onset frequencies seem to be lower by around 0.02 Hz. As mentioned previously, the value of the damping coefficient is known to limited precision, and this altered value is just as reasonable an estimate as the one we have used thus far.

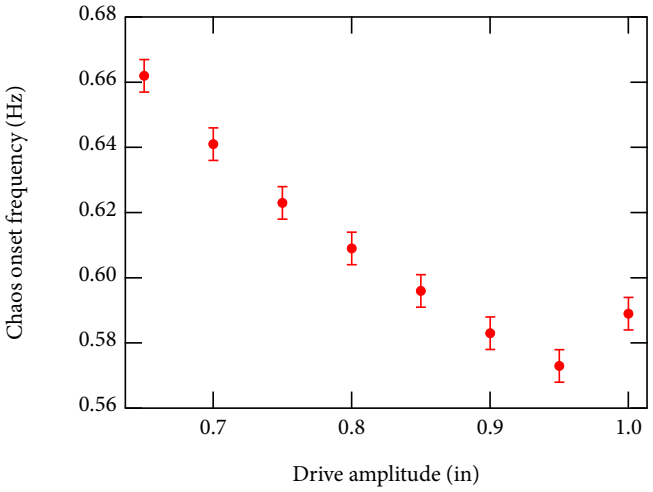

Figure 8: Plot of the frequencies at which chaotic behavior begins in the theoretical system with a damping constant of 0.00015 kg m/s.

5.2 Qualitative Comparison of Poincaré Plots

The Poincaré plots produced by our model were also compared to the Poincaré plots from the experimental setup in the Sophomore Lab. The Poincaré plots are shown in Figure 9. They appear qualitatively similar. It is possible that adjusting the damping constant as discussed above would improve the resemblance.

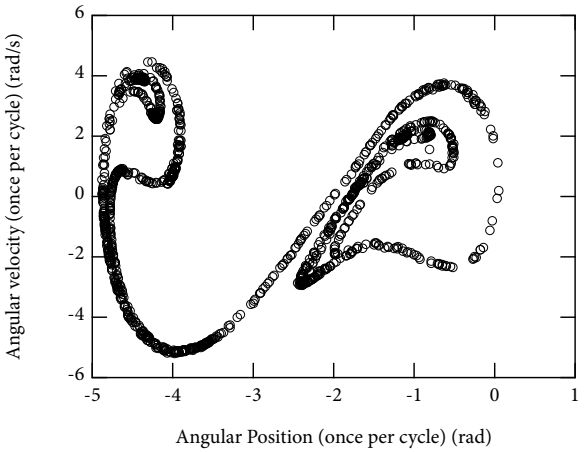

(a) 0.720 Hz, experimental data

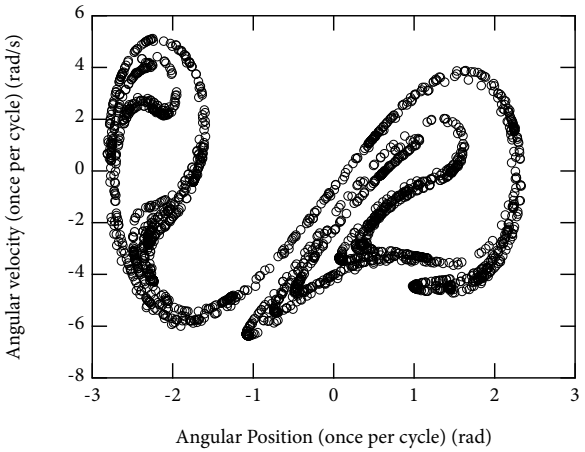

(b) 0.720 Hz, theoretical predictions

Figure 9: Comparison of experimental (a) and theoretical (b) Poincaré plots at a drive frequency of 0.720 Hz. The plots are qualitatively similar.

6 Conclusion

The behavior of a sinusoidally-driven chaotic pendulum has been investigated for a variety of drive frequencies. The system exhibits chaotic behavior, as shown in the phase plots, Poincaré plots, and bifurcation diagrams. Branching behavior was observed for frequencies just over those in the chaotic region. Feigenbaum's first constant was calculated from the model (with large uncertainty) and it seems at least plausible that the branching in the bifurcation plot obeys Feigenbaum's predictions.

The range of frequencies at which chaotic behavior was predicted to begin aligned well with the observed onset of chaos, but the drive amplitudes that generated these onset frequencies were offset by around 0.2 inches. This offset can be reduced by altering the damping constant. Poincaré plots determined theoretically and experimentally appeared at least qualitatively similar.

7 Appendix: Bifurcation Plots

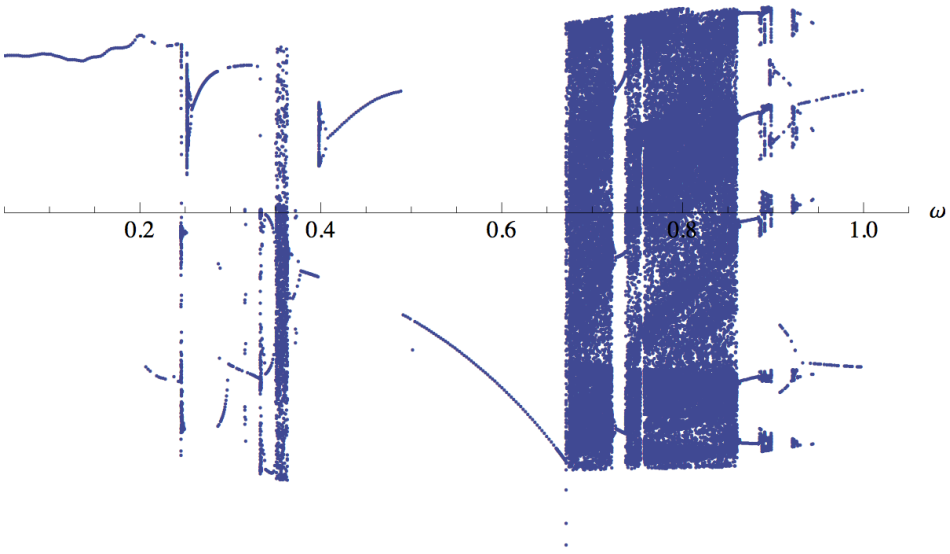

(a) Full frequency range

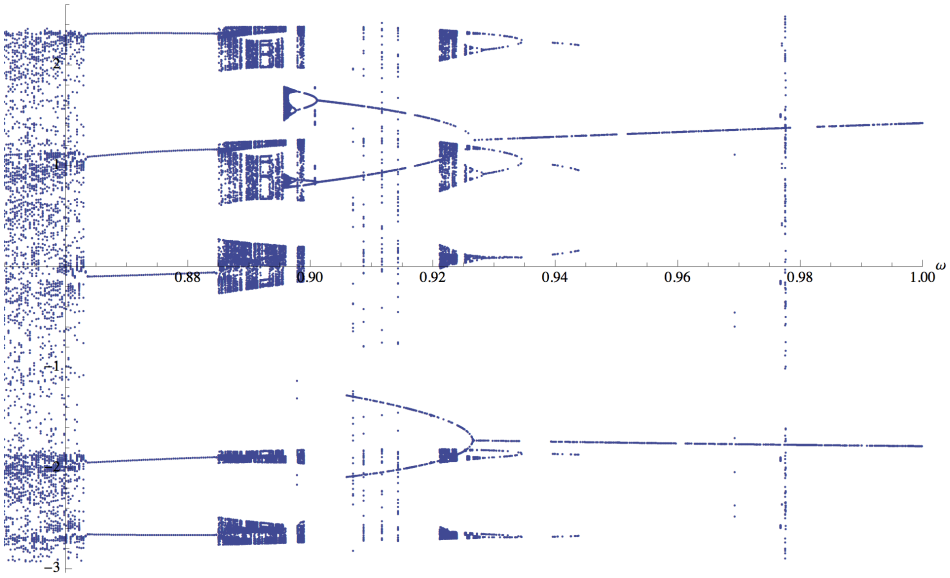

(b) Region of period doubling

Figure 10: Bifurcation diagrams over the full range of frequency (a) and a smaller region of interest (b).